

Mechanics of drag reduction of an axisymmetric body of revolution with shallow dimples

Journal Title
XX(X):1-10
©The Author(s) 2020
Reprints and permission:
sagepub.co.uk/journalsPermissions.nav
DOI: 10.1177/ToBeAssigned
www.sagepub.com/

J P PANDA, J HANDIQUE, H V WARRIOR

Abstract

In this article, the mechanics of drag reduction on an axisymmetric body of revolution by shallow dimples is presented by using the high-fidelity Reynolds Stress Modeling based simulations. Experimental results of drag evolution from published literature at different Reynolds numbers are used to validate the model predictions. The numerical predictions show good agreement with the experimental results. It is observed that the drag of the body is reduced by a maximum of 31% with such shape modification (for the depth to diameter ratio of 7.5% and coverage ratio of 52.8%). This arises due to the reduced level of turbulence, flow stabilization and suppression of flow separation in the boundary layer of the body. From the analysis of turbulence states in the anisotropic invariant map (AIM) for the case of the dimpled body, we show that the turbulence reaches an axisymmetric limit in the layers close to the surface of the body. There is also a reduced misalignment between the mean flow direction and principal axis of the Reynolds stress tensor, which results in such drag reduction. The dimple depth to diameter and coverage ratio are also varied to evaluate its effect on drag evolution.

Keywords

Drag reduction, Dimples, Computational Fluid Dynamics, Turbulence Modeling, Reynolds Stress Modeling

Introduction

The drag on an axisymmetric body arises either from the pressure of the fluid or from the fluid friction acting along its wetted surface. The major portion of the drag that acts in the direction opposite to the motion of the body is generated from the region that is very close to the boundary of the body where the flow is always turbulent. A detailed understanding of the turbulent flow, its control, the drag evolution and the mechanism of reduction of viscous drag along a body of engineering interest will lead to technological advancements in field of engineering design.

Drag reduction by flow control along axisymmetric bodies such as submarines and other underwater vehicles(Panda et al. 2020) can lead to optimized energy consumption and reduce the cost of operation (Frohnappfel et al. 2012). The viscous drag amounts to about 90% of the total drag of underwater bodies as reported in Frohnappfel et al.(Frohnappfel et al. 2007a). For aircrafts the drag can be controlled by delaying the laminar-turbulent boundary-layer transition. Sustained laminar flow over aircraft's wings, nacelles and tail surfaces can result in drag reduction. The methods of control of laminar-turbulent boundary layer transition include application of suction near the leading edge, minimization of leading edge surface roughness, reduction of leading edge sweep or by utilizing periodic discrete roughness elements in the spanwise direction(Saric et al. 2019). There are various flow control methods available by which drag over an axisymmetric body can be reduced.⁸²⁰⁰⁸Choi et al.Choi, Jeon, and Kim Frohnappfel et al. (Frohnappfel et al. 2007a) used surface embedded grooves for drag reduction. They observed that turbulence reaches an axisymmetric state over the grooved wall and the turbulence

fluctuations are highly suppressed in the boundary layer of the grooved wall, which resulted in significant drag reduction. Krieger et al.(Krieger et al. 2018) designed an anti-turbulence surface for maximum drag reduction in channel flows and observed a drag reduction of 60 percent lower than the flat surface. The main purpose of such an anti-turbulence surface is to damp the turbulence stresses in the near-wall flow layers. Watkins et al.(Watkins et al. 2017) used bio-inspired coatings to reduce drag of an AUV(Panda et al. 2020; Mitra et al. 2020). They mainly have used micro-fibres to modify the surface of the AUV and to suppress flow separation. Toonder et al.(Den Toonder et al. 1997) used polymer additives(Xi 2019) in turbulent pipe flow for reduction of drag. Itoh et al.(Itoh et al. 2006) used seal fur surface in a rectangular channel to check the drag reducing capability of the surface and observed a drag reduction of 12 percent. Degroot et al.(DeGroot et al. 2016) studied the drag reduction mechanics of a turbulent channel flow using stream-wise grooves.(Abderrahaman-Elena and García-Mayoral 2017) used an anisotropically permeable surface(Gómez-de Segura et al. 2018) for drag reduction. With increase in stream-wise permeability the drag was observed to be reduced. However, in their analysis it was noticed after certain value of permeability the drag reduction failed. The drag of an axisymmetric body can also be minimized by dimples. Such research started from the

Department of Ocean Engineering and Naval Architecture
Indian Institute of Technology, Kharagpur, India

Corresponding author:
J P Panda, IIT Kharagpur, INDIA
Email: jppanda@iitkgp.ac.in

aerodynamic studies on golf-balls. The golf-ball dimples can reduce the drag coefficient of a sphere by 50 percent(Choi et al. 2006). The drag coefficient can be defined as, $C_D = F_D / (0.5\rho U_0^2 A)$, here F_D is the drag force, U_0 is the free stream velocity, d is the diameter of the sphere, ρ is the density of the fluid and A is the cross-sectional area of the sphere.

There are numerous studies available in literature in which experimental and numerical studies are performed to study the flow characteristics over dimpled bodies(Tay et al. 2014) such as cylinders(Bearman and Harvey 1993), spheres(Choi et al. 2006) and for internal flow cases such as channels(Tay et al. 2015; Lienhart et al. 2008; Won et al. 2005; Ligrani et al. 2001). The effect of dimpling of a sphere on drag reduction was investigated in Choi et al.(Choi et al. 2006), where they observed the drag of the sphere was reduced as much as 50%, in comparison to the non-dimpled sphere. They also noticed that the reduced drag coefficient was nearly same for a certain range of Reynolds numbers. Tay et al.(Tay et al. 2015) observed that shallow dimples in a channel increase the stream-wise vorticity in the flow field. They considered two depth to diameter ratios of the dimples for their simulations. For a lower range of Reynolds numbers up to 35000, they observed a maximum drag reduction of 3 percent.

There are no such studies found in literature in which, the detailed flow dynamics and corresponding drag evolution over axisymmetric bodies of revolution(Kumar and Mahesh 2018; Posa and Balaras 2016, 2020; Mitra et al. 2019; Jiménez et al. 2010; Ashok et al. 2015; Posa and Balaras 2018; Bridges et al. 2003) such as submarine models with dimpled surface are analyzed. In this study, the detailed dynamics of turbulent flow evolution and its damping over an axisymmetric dimpled body is presented. Experimental results from published literature(Jagadeesh et al. 2009) for the case of the non-dimpled body are used to validate the numerical model predictions. A series of numerical simulations based on high fidelity Reynolds stress models are performed for analyzing the effect of variation of depth to diameter ratio and coverage area to total surface area ratios on drag evolution along the axisymmetric body. The turbulence structure in the form of Reynolds stress tensor are presented along the body and finally anisotropy invariant map is used to demarcate the state of turbulence for the smooth and dimpled body.

Numerical modeling

The present numerical setup consists of a model of an axisymmetric underwater body Fig. 1. Basically, the model is a predecessor of the DARPA suboff submarine model(Huang et al. 1978; Groves et al. 1989). The length and maximum diameter of the model are 1.4 and 0.14 meters respectively. The detailed dimensions of the model are available in(Huang et al. 1978). The mid-section of the body was dimpled over a length of 0.7m (starting from 0.25m to 0.95 meter from the beginning towards the end) to check its effect on corresponding drag reduction. The surface diameter of the dimple is taken as 14mm. The depth of the dimple is varied by changing the depth to surface diameter ratios from 2.5 to 7.5 percent. The depth to surface diameter ratios are not

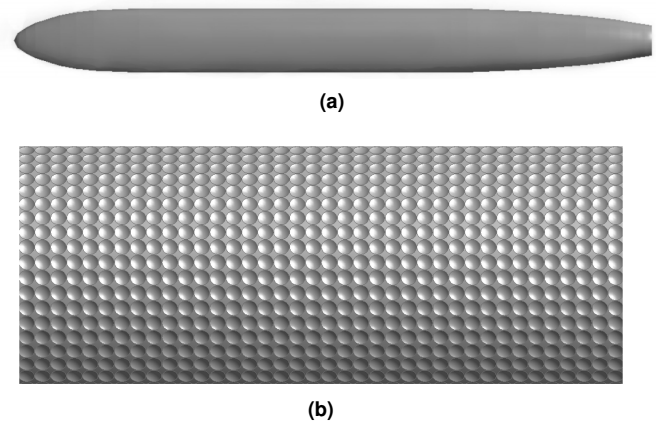


Figure 1. a) Geometry of the axisymmetric body of revolution(non-dimpled), which has similar shape as of DARPA SUBOFF model(Groves et al. 1989) developed by (Huang et al. 1978; Groves et al. 1989) b) The dimpled body with magnified mid-section.

increased further since that can adversely affect the strength of the body. The coverage ratio of the dimples were also varied to check its effect on drag evolution. In the numerical analysis x , y and z correspond to stream-wise, vertical and span-wise directions respectively. The velocities are u , v and w in the x , y and z directions respectively.

For the numerical simulations, a key criterion is the selection of the turbulence model. Turbulence models are simplified closures that seek to relate complex, high order quantities such as the Reynolds stress, in terms of lower-order quantities like the mean rate of strain, etc. There are many different turbulence modeling approaches available, such as 1-equation models, eddy viscosity based models, Reynolds stress models, etc and numerous models within each approach. The use of eddy viscosity based models, such as the $k - \epsilon$ and $k - \omega$ models is the norm in industrial simulations of turbulent flows, due to their lower computational expense, computational stability and robustness. In this investigation, we utilize the Reynolds Stress Models (RSM)(Speziale et al. 1991) to predict the turbulence damping and corresponding drag reduction over the dimpled body. The central difference between the approach of eddy viscosity based models and Reynolds stress closures lies in their computation of the Reynolds stress tensor. Eddy viscosity based approaches use the conceptualization of a turbulent viscosity to relate the turbulent kinetic energy to the instantaneous mean rate of strain. On the other hand, Reynolds Stress Models explicitly solve the transport equations for the evolution of individual components of the Reynolds stress tensor (Pope 2001). Due to this eddy viscosity hypothesis, eddy viscosity based models are unable to correctly capture the anisotropy of turbulent flows and thus, replicate the directional effects of turbulence (Mompean et al. 1996; Mishra and Girimaji 2019; Sjögren and Johansson 2000). Similarly, they are unable to adhere to physically permissible solutions for many complex flows (Mishra and Girimaji 2014). In such cases, Reynolds Stress Models offer better performance as they explicitly compute the transport of the Reynolds stress tensor components. However, a key assumption of eddy viscosity based turbulence models is that the eigen-directions of the

Reynolds stress tensor are perfectly aligned with those of the mean rate of strain (Mishra and Girimaji 2015). While this alignment is not true for most cases of complex turbulent flow, this misalignment is even more pronounced for regions where flow separation and reattachment occur. As a result for turbulent flows with flow separation and reattachment eddy viscosity models often give unsatisfactory results (Craft et al. 1996). Similarly eddy viscosity models assume that the Reynolds stress tensor forms an adequate basis to describe the state of the turbulent flow field (Mishra et al. 2016). This assumptions leads to discrepancies in the model predictions for complex turbulent flows of engineering interest (Mishra et al. 2019). In investigations, the use of eddy viscosity based models for turbulent flow separation problems has led to substantial errors in the prediction of the location of flow separation, the location of flow reattachment and the size of the separation bubble. These inaccuracies have cascading effects on the model's predictions of the forces on the body, including the drag forces on the body. Such flow separation and reattachment are a primary focus of our study as they have a seminal effect of the drag over a body. In this light we utilize the Reynolds Stress Modeling approach in our investigation.

In summary, RSM based models (Panda 2020; Warrior et al. 2014) have higher potential to replicate the complex flow physics (Manceau et al. 2014) over the dimpled body in comparison to the eddy viscosity models (Pope 2001) (eddy viscosity models are known to be unreliable for flows with separation, strong pressure gradient and curvature), since RSM does not rely on simplifying assumptions in defining the Reynolds stress in term of the local flow parameters, rather directly employ equations for the Reynolds stress components (Panda et al. 2017; Mishra and Girimaji 2013) and one scale determining equation in the flow field and to predict the flow evolution mechanism and by using such models the complete structure of turbulence in terms of the Reynolds stress components can be obtained directly (Mishra and Girimaji 2017; Panda 2019). The predictive capability of such models for flow along cylinders is validated in (Monte et al. 2011), which shows the predictions are quite satisfactory for a wide range of Reynolds numbers. In contrast to direct numerical simulations and large-eddy simulations (Posa and Balaras 2020; Kumar and Mahesh 2018) (for LES, Kumar and Mahesh (Kumar and Mahesh 2018) have used 8192 processors to simulate the flow past an axisymmetric body of revolution) the computational cost is very less.

The modeled transport equation for the Reynolds stress can be written as (Panda and Warrior 2018; Mishra and

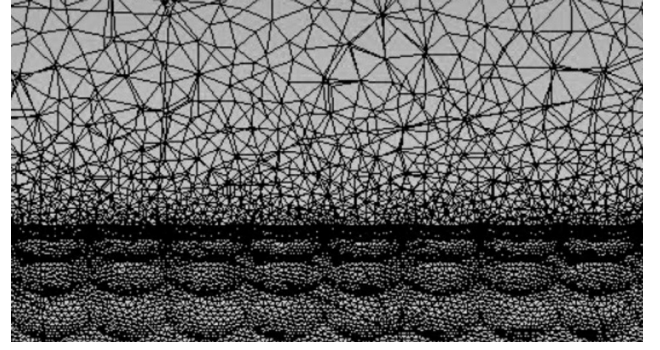


Figure 2. Mesh in local region around the dimpled AUV.

Girimaji 2010):

$$\begin{aligned} \partial_t \overline{u_i u_j} + U_k \frac{\partial \overline{u_i u_j}}{\partial x_k} &= P_{ij} - \frac{\partial T_{ijk}}{\partial x_k} - \eta_{ij} + \phi_{ij}, \\ \text{where,} \\ P_{ij} &= -\overline{u_k u_j} \frac{\partial U_i}{\partial x_k} - \overline{u_i u_k} \frac{\partial U_j}{\partial x_k}, \\ T_{kij} &= \overline{u_i u_j u_k} - \nu \frac{\partial \overline{u_i u_j}}{\partial x_k} + \delta_{jk} \overline{u_i p} + \delta_{ik} \overline{u_j p}, \\ \eta_{ij} &= -2\nu \overline{\frac{\partial u_i}{\partial x_k} \frac{\partial u_j}{\partial x_k}}, \\ \phi_{ij} &= \overline{\frac{p}{\rho} \left(\frac{\partial u_i}{\partial x_j} + \frac{\partial u_j}{\partial x_i} \right)} \end{aligned} \quad (1)$$

In equation 1, P_{ij} denotes the turbulence production, the diffusive transport is denoted as T_{ijk} , ϵ_{ij} : dissipation rate tensor and ϕ_{ij} : pressure strain correlation. The complex flow physics resulting from flow over dimpled surfaces can be accurately captured by a standard pressure strain correlation model. For the present simulations, the linear model of (Speziale et al. 1991) is used, in which the pressure strain correlation has the form:

$$\begin{aligned} \phi_{ij}^{(R)} &= (C_1 - C_1^* II^{0.5}) K S_{ij} + \\ &C_2 K (b_{ik} S_{jk} + b_{jk} S_{ik} - 2/3 b_{mn} S_{mn} \delta_{ij}) \\ &+ C_3 K (b_{ik} W_{jk} + b_{jk} W_{ik}) \end{aligned} \quad (2)$$

Following standard practice, the closure coefficients are taken as $C_1 = 0.8$, $C_1^* = 1.3$, $C_2 = 1.25$ and $C_3 = 0.4$, as is outlined in the original study.⁵⁸¹⁹⁹¹Speziale et al. Speziale, Sarkar, and Gatski

In order to study the effect of the dimpling of the axisymmetric body, we performed numerical simulations of the physical problem under consideration. A rectangular three dimensional solution domain is constructed over the body. The governing equations are solved by using a finite volume method (Anderson and Wendt 1995). The no-slip and no-penetration boundary conditions are applied at the walls. A line-by-line tridiagonal matrix element algorithm (TDMA) is used for solving the discretized system of linear algebraic equations. A fully implicit scheme is used for the time integration. The semi-implicit method for pressure linked equations (SIMPLE) is used for the pressure velocity coupling. A more densely spaced grid is used close to the wall of the axisymmetric body as shown in Fig.2. We had used unstructured mesh in our simulations. A mesh

sensitivity study is conducted for four different meshes with successive refinement leading to an increase in the total number of cells in the flow domain. For the meshes utilized the total number of cells in the domain were 0.9 Million, 1.8 Million, 2.5 Million and 3.5 Million, respectively. We find that the quantities of interest calculated using the final two levels of mesh refinement do not show appreciable changes and consequently, we utilize the mesh with 2.5 Million elements in the results of this investigation.

While using wall functions with Reynolds Stress Models, the best practice guidelines (Fluent 2015; Salim et al. 2010; Ariff et al. 2009) for simulations outline that the y^+ value should be in the range $30 < y^+ < 300$. Since the Reynolds stress model was used for the numerical simulations with the wall functions, the values of y^+ for the four meshes utilized in the mesh independence study were calculated to be 190, 130, 70 and 40 respectively. The corresponding first layer thickness for the three different meshes was calculated accordingly. For y^+ values 190, 130, 70 and 40, the drag coefficient values are 0.0315, 0.0326, 0.0382 and 0.0383 respectively, for the Reynolds number 3.67×10^5 , (the drag coefficient from the experimental data for the same conditions was 0.0389). The drag coefficient values predicted with the mesh of 2.5 Million cells matches well with experimental results of (Jagadeesh et al. 2009) for all six Reynolds numbers (ranging from 1.05×10^5 to 3.75×10^5). The RSM predictions of drag coefficients are presented for different Reynolds numbers with solid lines in fig. 3. Experimental results of (Jagadeesh et al. 2009) are shown in dotted lines. The numerical predictions are in good agreement with the experimental results. In all the numerical simulations the solution has been iterated till convergence at each time step.

Results and discussion

Effect of dimpling of the body on drag reduction

Fig. 4a shows the variation of velocity in the vertical direction over the body. The velocity was non-dimensionalized with respect to the corresponding free stream velocity. From the reduced slope of velocity profile over the dimpled body, it is clear that flow stabilization is manifested as observed in the investigation of Posa and Balaras (Posa and Balaras 2020). The magnitude of x-velocity is decreasing, because of the interaction of eddies generated by dimples with the longitudinal vortices in the streamwise direction. The larger slope of the velocity profile for the non-dimpled body signifies the rapid production of turbulence in the boundary layer. An analysis of velocity component in the radial (wall normal) direction (Fig. 4b) reveals that, for the case of non-dimpled body in the regions very close to the wall, the wall normal velocity is negative, which signifies the existence of flow separation. However, for the dimpled body the wall normal velocity is positive, this give insights into the mechanism by which the dimpled body suppress the flow separation.

In the turbulent boundary layer, the existence of wall-normal vertical fluid structures (eddies) are the main source of skin friction drag as reported in (Fukagata et al. 2002; Robinson 1991). These are associated with a larger magnitude of wall-normal vorticity and the higher vorticity is generated by the interaction of the large eddies with the

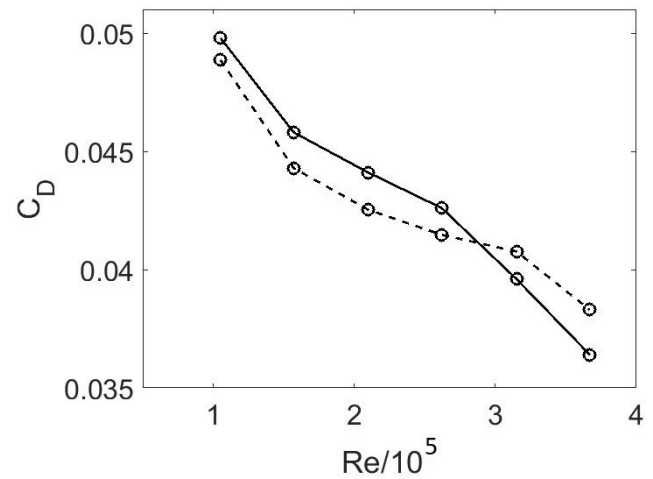


Figure 3. Variation of drag coefficient with Reynolds numbers, the dashed and solid lines correspond to the RSM predictions and the experimental results of (Jagadeesh et al. 2009) respectively.

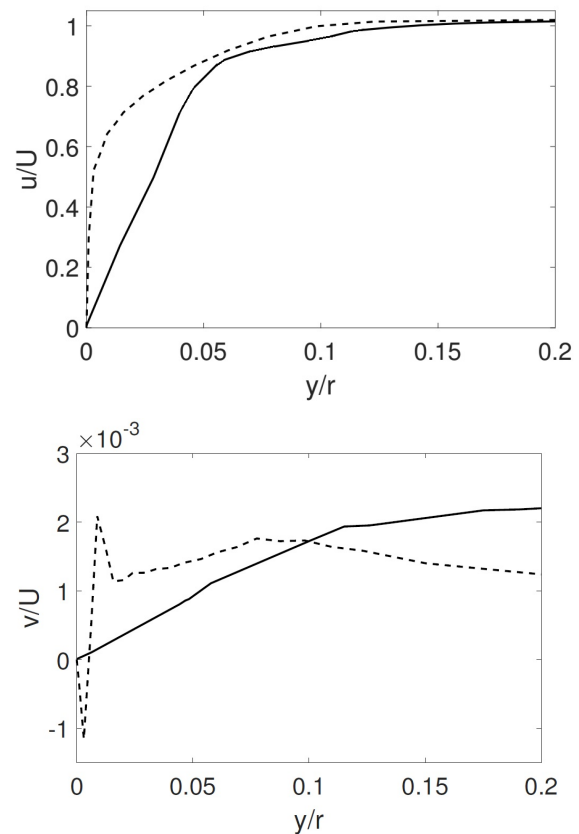


Figure 4. Comparison of the velocity distribution for dimpled (solid line) and non-dimpled body (dashed line). The data were taken at $x/r=8.5$ (at the beginning of the body $x/r=0$).

wall of the axisymmetric body. In figure 5 the variation of wall-normal vorticity is presented. The solid and dashed line corresponds to the vorticity distribution for the dimpled and non-dimpled bodies respectively. There is a reduction of the wall-normal vorticity for the dimpled body since the dimples act as large eddy break-up (LEBU) devices (Choi et al. 1994), which breaks the larger turbulence generating eddies into smaller dissipative eddies in layers very close to

the body resulting in a net reduction of turbulent energy of eddies for interaction with the wall. For the dimpled body, as shown in figure 5 the wall-normal vorticity is mainly reduced in the layers very close to the wall of the body, which signifies that the near-wall coherent structures has a larger effect on the skin friction drag evolution along the body. Dimples mainly provide suction effect and dampen the coherent structures(Park and Choi 1999).

The distribution of turbulence/Reynold shear stress is shown in Fig. 6. From the figure it is clear that there is a sharp decrease in the turbulence shear stress, because of the flow damping and stabilization over the dimpled surface. The dimple array mainly suppresses the formation and interaction of wall-normal eddies by generating stream-wise vorticity into the flow field(Tay et al. 2015).

The turbulence shear stress R_{12} has a direct relationship with the skin friction evolution along axisymmetric bodies:⁴¹²⁰¹¹Monte et al.Monte, Sagaut, and Gomez

$$C_f^T = \frac{1}{f(a)} \int_a^{a+1} (1+a-y)(-R_{12})ydy \quad (3)$$

where a is the radius of the axisymmetric body and $f(a) = a/2(11/24 - a/6)$ is a shape factor. In the formulation of the turbulent skin friction C_f^T , The Reynolds stress is weighted by $1+a-y$, which signifies that the near wall turbulence structures have a larger contribution on the skin friction evolution. The reduction in turbulence stresses resulted in skin friction drag reduction, and the total drag of the body is reduced(Choi et al. 1994).

The Reynolds shear stress can be decomposed in terms of the Reynolds stress anisotropy tensor(Monte et al. 2011). When considering the rotation of an angle β such as b_{ij} is diagonal, D_{kl} ,

$$b_{ij} = p_{ik}D_{kl}P_{lj}, \text{ where } P = \begin{pmatrix} \cos\beta & \sin\beta & 0 \\ \sin\beta & \cos\beta & 0 \\ 0 & 0 & 1 \end{pmatrix}$$

The Reynolds shear stress can be expressed as a function of angle β , the first two eigenvalues of the Reynolds stress anisotropy tensor and the turbulence kinetic energy(Monte et al. 2011),

$$-R_{12} = -k(\lambda_2 - \lambda_1)\sin 2\beta. \quad (4)$$

As described in (Monte et al. 2011), the reduction of angle β has a direct effect on the skin friction drag evolution along the body. The reduction of β signifies a reduced misalignment between the mean flow direction and the main axis of the Reynolds stress. As shown in figure 7 there is a sharp reduction in the angle β with y/r in the boundary layer of the dimpled body.

For an accurate description of turbulence damping over the dimpled body, the variation of turbulence kinetic energy over a horizontal line along the length of the body in the boundary layer (at $y/r=0.07$) is plotted in fig.8. It is noticed that the turbulence along the body is decaying similar to the pattern observed in grid generated turbulence(Panda et al. 2018). However, a reverse trend of turbulence evolution is observed over the non-dimpled body, where turbulence is found to be increasing along the length of the body.

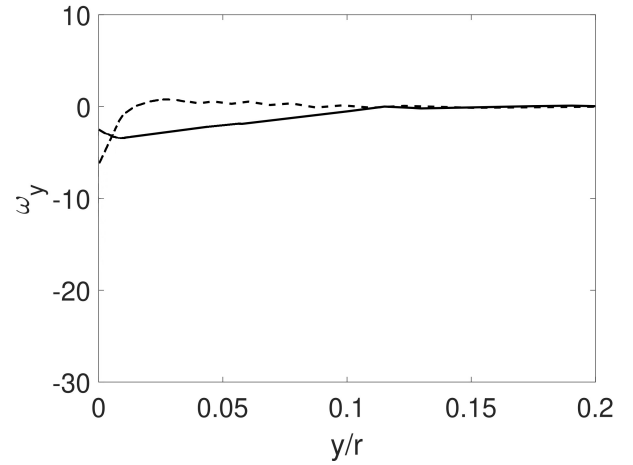


Figure 5. Comparison of the wall normal vorticity (along the y -direction) distribution for dimpled (solid line) and non-dimpled (dashed line) body.

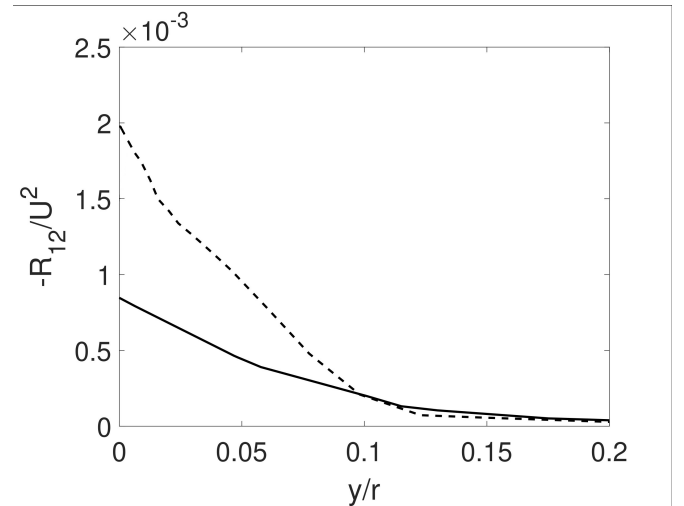


Figure 6. The distribution of Reynolds shear stress in the boundary layer of the axisymmetric body. The solid and dashed line correspond to dimpled and non-dimpled bodies respectively.

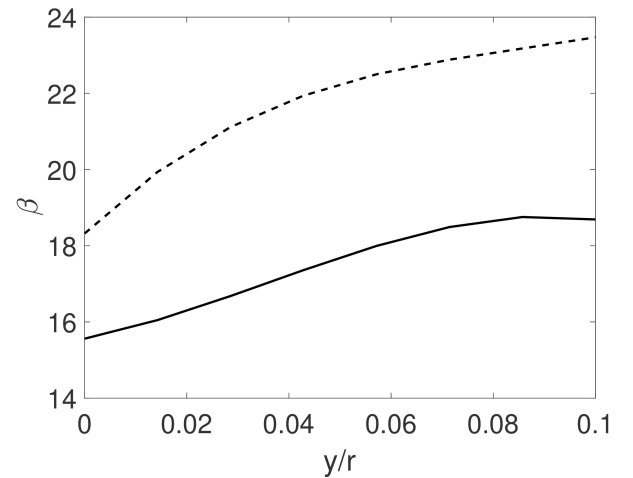


Figure 7. The variation of angle β in the boundary layer of the body. The solid and dashed line correspond to dimpled and non-dimpled bodies respectively.

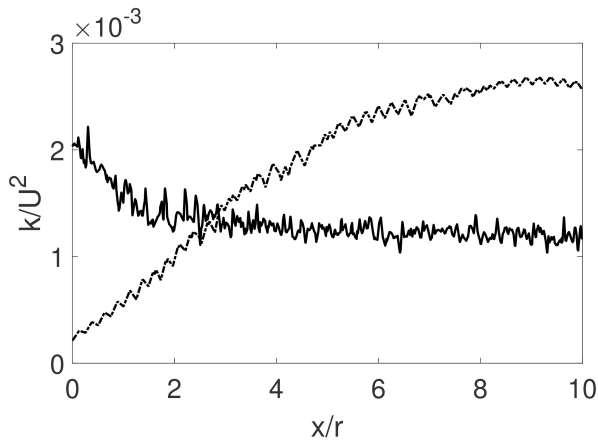


Figure 8. Evolution of turbulence kinetic energy along the length of the body, for $y/r=0.07$. The solid and dashed-dot line correspond to dimpled and non-dimpled bodies respectively. A decay of turbulence kinetic energy is noticed along the length of the dimpled body.

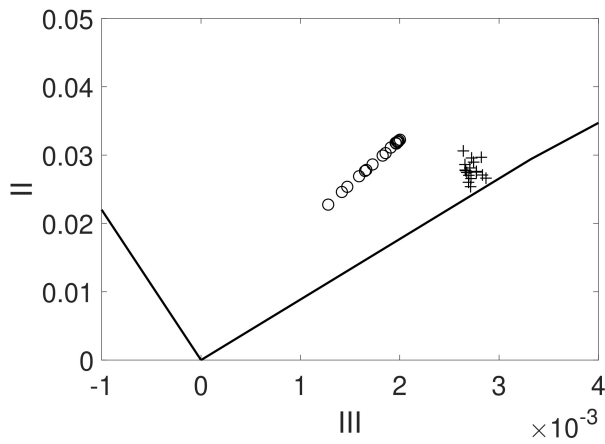


Figure 9. The anisotropy invariant map representing different states of turbulence. The circles and plus symbols represent turbulence states over non-dimpled and dimpled body respectively. The data were taken at different stream-wise locations along the body (for $y/r=0.07$).

Krieger et al. (Krieger et al. 2018) observed that turbulence satisfies statistical axisymmetry in the velocity fluctuations and one component state in the near-wall region, over the anti-turbulence surfaces. The different states of turbulence (such as one component or two component) along the body can be visualized by anisotropy invariant map (AIM) (Lumley 1979), with the second ($= -b_{ii}^2/2$) and third invariants ($= b_{ii}^3/3$) of the Reynolds stress anisotropy ($b_{ij} = R_{ij}/2k - 1/3\delta_{ij}$). R_{ij} is the Reynolds stress tensor. From the AIM paths of turbulence reported in figure 9, it is observed that the turbulence over the dimpled body shows a higher degree of axisymmetric character, as all the plus symbols in the AIM figure approaches toward the right side of the AIM where the Reynolds stress ellipsoid corresponds to rod-like axisymmetric states (Simonsen and Krogstad 2005). This is in accordance to the findings of (Frohnafel et al. 2007b), where they noticed that for drag reduced flows the near wall turbulence approaches towards one component limit. However, the turbulence over the non-dimpled body is far from the axisymmetric state.

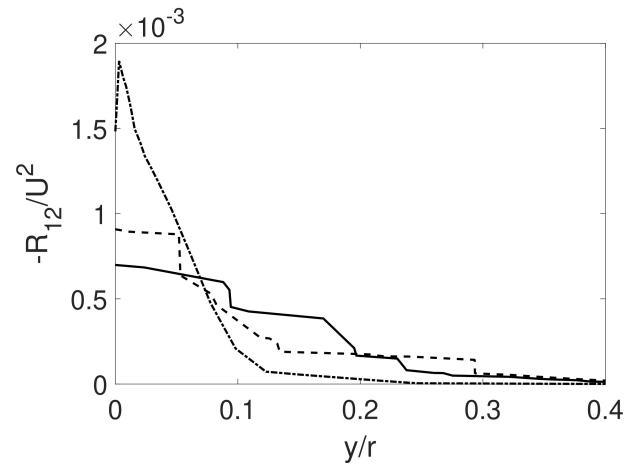


Figure 10. The distribution of Reynolds shear stress in the boundary layer of the axisymmetric body. The dashed, dashed-dot and solid lines correspond to 2.5, 5 and 7.5 percent depth to diameter (s/d) ratios respectively.

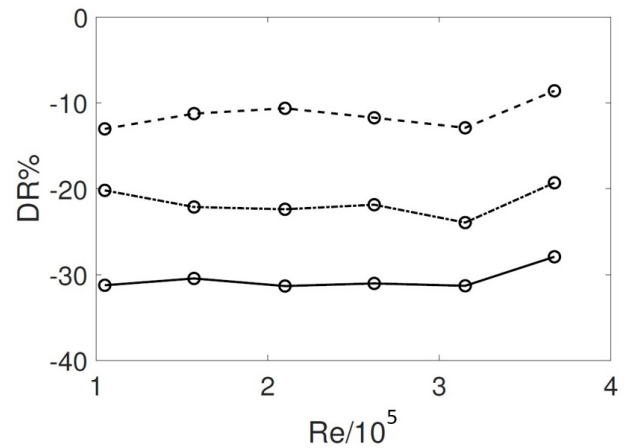


Figure 11. Drag reduction achieved with micro-dimples, the dashed, dashed-dot and solid lines correspond to 2.5, 5 and 7.5 percent depth to diameter (s/d) ratios respectively.

Effect of depth to diameter (s/d) ratio on drag reduction

To analyze the effect of the ratio of depth (s) to surface diameter (d) of the dimple shape on the turbulence evolution along the axisymmetric body of revolution, this s/d ratio is varied from from 2.5 percent to 7.5 percent. This ratio describes the aspect ratio of the dimple and is a characteristic of its geometry. As reported in literature for the case of dimpled channel flow (Tay et al. 2015), further increase in s/d ratio may result in flow separation, that may enhance drag.

The variation of Reynolds shear stress is presented in Fig. 10. The dashed, dashed-dot and solid lines correspond to the turbulence stresses for s/d ratios 2.5, 5 and 7.5 percents respectively. With increase in s/d ratio from 2.5 to 5 percent, a decrease in turbulence stresses in all three components of the turbulence stresses are noticed, However with further increase in s/d ratio, an increase in Reynolds stress components at upper layers starting from y/r ratios 0.06 to 0.3 is observed. Consequently it is not advisable to increase the depth of the dimple further, which may enhance the turbulence level further and will result in drag increase,

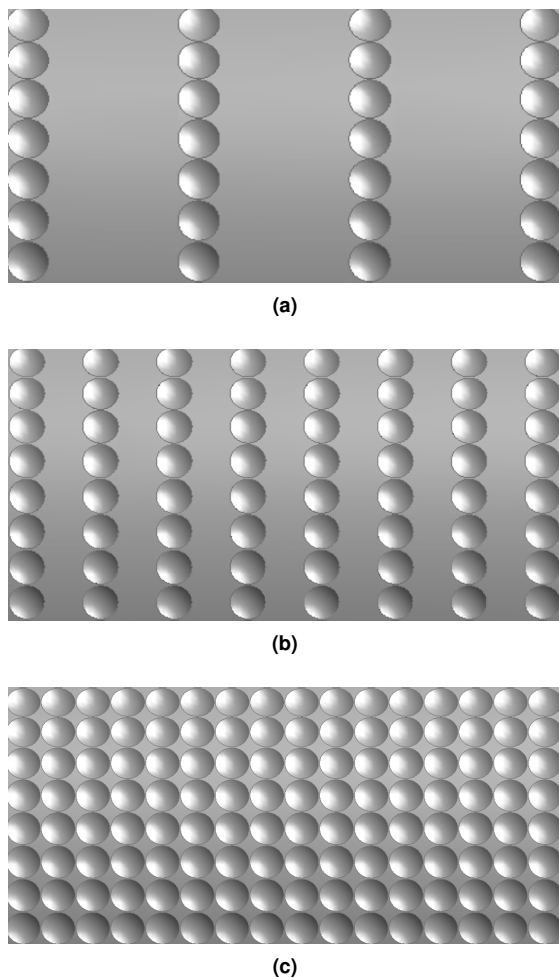


Figure 12. Dimpling of the body for coverage area variation. only a magnified portion is provided. Dimensions not to scale. a) $a/A=13.2$ percent, b) $a/A=26.4$ percent, c) $a/A=52.8$ percent respectively.

which is undesirable. Although, the turbulence level is higher for a range of y/r ratios for s/d equals to 7.5 percent, a over all drag reduction is achieved at all the Reynolds numbers in Fig. 11, since turbulence level at the layers close to the body is less in comparison to the other two s/d ratios. This depict the fact that, the near wall turbulence structure has larger effect on viscous drag evolution in comparison to the free stream turbulence for the flow along axisymmetric bodies. In Fig. 11 the net drag reduction percentage for different values of depth to diameter ratio of the dimples are presented. The negative sign in the figure signifies that the drag is reducing with the use of the dimpled surface. An increase in drag reduction was noticed with an increase in depth to diameter ratios. Maximum drag reduction was observed for the depth to diameter ratio of 7.5 percent (31 percent). The depth to diameter was not enhanced further since that can have an adverse effect on the strength of the body. (Choi et al. 2006) had observed a drag reduction of 50 percent for dimpled spheres, the drag reduction of the present axisymmetric body can further enhanced by applying dimples over the entire surface area of the body.

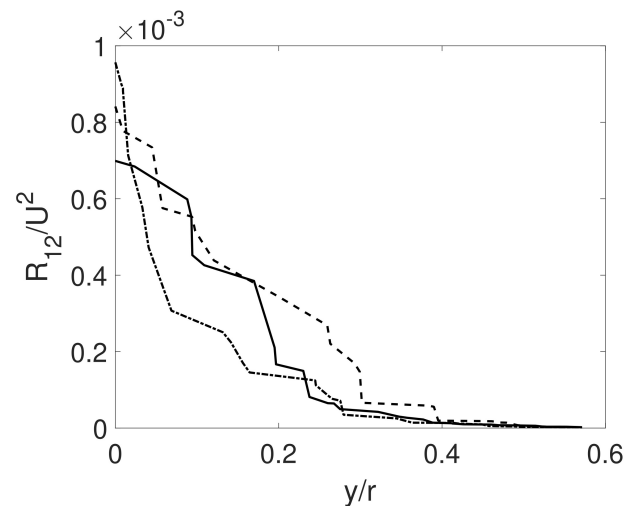


Figure 13. The distribution of Reynolds stress components in the boundary layer of the axisymmetric body. The dashed, dashed-dot and solid lines correspond to 13.2, 26.4 and 52.8 a/A ratios respectively.

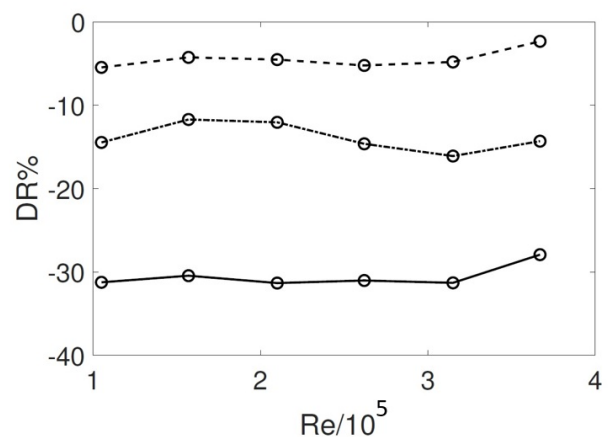


Figure 14. The drag reduction achieved with different a/A ratio. Dashed, dashed-dot and solid lines correspond to 13.2, 26.4 and 52.8 a/A ratios respectively.

Effect of coverage ratio (a/A) on drag reduction

The coverage ratio(a/A) can be defined as the ratio of area occupied by dimples(a =total number of dimples multiplied by area occupied by one dimple over the body) divided by the total surface area of the body over which dimples were made. Accordingly three different a/A ratios (13.2, 26.4 and 52.8 percent) are considered in the simulations as shown in Fig. 12. For varying the coverage ratio, the dimple densities were varied only along the length of the body as shown in Fig. 12. The dimple densities in the circumferential direction were not varied.

In Fig. 13 the variation of turbulence stresses for different coverage ratios are presented. A similar trend of trend of turbulence evolution (as of s/d variation) is observed for different coverage ratios. With increase in coverage ratio from 13.2 percent to 26.4, all the three components of turbulence stresses near the wall was found to be increasing, however, the stresses at the layers above $y/r=0.02$ turbulence level was very less. With further increase in a/A ratio a decrease in near wall turbulence was observed. This is clear

that both near wall and far wall turbulence contributions has effect on the viscous drag evolution.

Concluding remarks

The reduction of drag on bodies is an critical line of research for engineering design as it may lead to better performance and efficiency. In this article, the mechanics of drag reduction of an axisymmetric body of revolution with shallow dimples have been presented. The effect of dimpling of the body on the evolution of turbulence structure along the body was analyzed. It was observed that the dimples have the ability to suppress the turbulence intensity in the boundary layer of the body, which resulted in a maximum drag reduction of 31 percent. Additionally the dimples on the surface lead to a change in the componentiality of the flow field evidenced in the state of turbulent flow anisotropy. From the anisotropy invariant map it was observed that due to this modification the state of turbulence componentiality transitions closer to the axisymmetric state, in the boundary of the body and over the dimpled body the turbulence was found to be decaying similar to the pattern observed in decaying grid turbulence. With variation of depth to diameter ratio of dimples, the near wall turbulence level was decreased, so an decrease in drag coefficient was noticed. A similar turbulence and drag evolution pattern was observed for coverage ratio variations. The s/d and a/A ratio were not increased further, since those may reduce the strength of the body. This is undesirable, since underwater bodies often cruise in marine environments where operating pressure is very high. Here we recommend s/d and a/A ratios 7.5 and 50 percent respectively, for safer operations in Naval Engineering applications. A detailed analysis based on strength of the body will be more appropriate for such recommendations, which can be considered as an future course of work.

References

- Nabil Abderrahaman-Elena and Ricardo García-Mayoral. Analysis of anisotropically permeable surfaces for turbulent drag reduction. *Physical Review Fluids*, 2(11):114609, 2017.
- John David Anderson and J Wendt. *Computational fluid dynamics*, volume 206. Springer, 1995.
- Mohd Ariff, Slim M Salim, and Siew Cheong Cheah. Wall y^+ approach for dealing with turbulent flow over a surface mounted cube: Part 1-low reynolds number. In *Seventh International Conference on CFD in the Minerals and Process Industries, Australia*, page 053001, 2009.
- Anand Ashok, Tyler Van Buren, and AJ Smits. Asymmetries in the wake of a submarine model in pitch. *Journal of Fluid Mechanics*, 774:416–442, 2015.
- PW Bearman and JK Harvey. Control of circular cylinder flow by the use of dimples. *AIAA journal*, 31(10):1753–1756, 1993.
- David H Bridges, James N Blanton, Wesley H Brewer, and Joel T Park. Experimental investigation of the flow past a submarine at angle of drift. *AIAA journal*, 41(1):71–81, 2003.
- Haecheon Choi, Parviz Moin, and John Kim. Active turbulence control for drag reduction in wall-bounded flows. *Journal of Fluid Mechanics*, 262:75–110, 1994.
- Haecheon Choi, Woo-Pyung Jeon, and Jinsung Kim. Control of flow over a bluff body. *Annu. Rev. Fluid Mech.*, 40:113–139, 2008.
- Jin Choi, Woo-Pyung Jeon, and Haecheon Choi. Mechanism of drag reduction by dimples on a sphere. *Physics of Fluids*, 18(4):041702, 2006.
- TJ Craft, BE Launder, and K Suga. Development and application of a cubic eddy-viscosity model of turbulence. *International Journal of Heat and Fluid Flow*, 17(2):108–115, 1996.
- CT DeGroot, C Wang, and JM Floryan. Drag reduction due to streamwise grooves in turbulent channel flow. *Journal of Fluids Engineering*, 138(12):121201, 2016.
- JMJ Den Toonder, MA Hulsen, GDC Kuiken, and FTM Nieuwstadt. Drag reduction by polymer additives in a turbulent pipe flow: numerical and laboratory experiments. *Journal of Fluid Mechanics*, 337:193–231, 1997.
- ANSYS Fluent. Ansys fluent. *Academic Research. Release*, 14, 2015.
- Bettina Frohnafel, Jovan Jovanović, and Antonio Delgado. Experimental investigations of turbulent drag reduction by surface-embedded grooves. *Journal of Fluid Mechanics*, 590:107–116, 2007a.
- Bettina Frohnafel, P Lammers, J Jovanović, and Franz Durst. Interpretation of the mechanism associated with turbulent drag reduction in terms of anisotropy invariants. *Journal of Fluid Mechanics*, 577:457–466, 2007b.
- Bettina Frohnafel, Yosuke Hasegawa, and Maurizio Quadrio. Money versus time: evaluation of flow control in terms of energy consumption and convenience. *Journal of Fluid Mechanics*, 700:406–418, 2012.
- Koji Fukagata, Kaoru Iwamoto, and Nobuhide Kasagi. Contribution of reynolds stress distribution to the skin friction in wall-bounded flows. *Physics of Fluids*, 14(11):L73–L76, 2002.
- Garazi Gómez-de Segura, Akshath Sharma, and R García-Mayoral. Turbulent drag reduction using anisotropic permeable substrates. *Flow, Turbulence and Combustion*, 100(4):995–1014, 2018.
- Nancy C Groves, Thomas T Huang, and Ming S Chang. Geometric characteristics of darpa (defense advanced research projects agency) suboff models (dtrc model numbers 5470 and 5471). Technical report, David Taylor Research Center Bethesda MD Ship Hydromechanics Dept, 1989.
- TT Huang, N Santelli, and G Belt. Stern boundary-layer flow on axisymmetric bodies. In *Twelfth symposium on naval hydrodynamics*, pages 125–167, 1978.
- Motoyuki Itoh, Shinji Tamano, Ryo Iguchi, Kazuhiko Yokota, Norio Akino, Ryutaro Hino, and Shinji Kubo. Turbulent drag reduction by the seal fur surface. *Physics of Fluids*, 18(6):065102, 2006.
- P Jagadeesh, K Murali, and VG Idichandy. Experimental investigation of hydrodynamic force coefficients over auv hull form. *Ocean engineering*, 36(1):113–118, 2009.
- Juan M Jiménez, Marcus Hultmark, and Alexander J Smits. The intermediate wake of a body of revolution at high reynolds numbers. *Journal of Fluid Mechanics*, 659:516–539, 2010.
- V Krieger, R Perić, J Jovanović, H Lienhart, and A Delgado. Toward design of the antiturbulence surface exhibiting maximum drag reduction effect. *Journal of Fluid Mechanics*, 850:262–303, 2018.

- Praveen Kumar and Krishnan Mahesh. Large-eddy simulation of flow over an axisymmetric body of revolution. *Journal of Fluid Mechanics*, 853:537–563, 2018.
- Hermann Lienhart, Michael Breuer, and Cagatay Köksoy. Drag reduction by dimples?—a complementary experimental/numerical investigation. *International Journal of Heat and Fluid Flow*, 29(3):783–791, 2008.
- PM Ligrani, JL Harrison, GI Mahmmmod, and ML Hill. Flow structure due to dimple depressions on a channel surface. *Physics of fluids*, 13(11):3442–3451, 2001.
- John L Lumley. Computational modeling of turbulent flows. In *Advances in applied mechanics*, volume 18, pages 123–176. Elsevier, 1979.
- Rémi Manceau, R Perrin, M Hadžiabdić, and S Benhamadouche. Investigation of the interaction of a turbulent impinging jet and a heated, rotating disk. *Physics of Fluids*, 26(3):035102, 2014.
- Aashwin A Mishra and Sharath S Girimaji. Pressure–strain correlation modeling: towards achieving consistency with rapid distortion theory. *Flow, turbulence and combustion*, 85(3-4): 593–619, 2010.
- Aashwin A Mishra and Sharath S Girimaji. Intercomponent energy transfer in incompressible homogeneous turbulence: multi-point physics and amenability to one-point closures. *Journal of Fluid Mechanics*, 731:639–681, 2013.
- Aashwin A Mishra and Sharath S Girimaji. On the realizability of pressure–strain closures. *Journal of fluid mechanics*, 755: 535–560, 2014.
- Aashwin A Mishra and Sharath S Girimaji. Hydrodynamic stability of three-dimensional homogeneous flow topologies. *Physical Review E*, 92(5):053001, 2015.
- Aashwin A Mishra and Sharath S Girimaji. Toward approximating non-local dynamics in single-point pressure–strain correlation closures. *Journal of Fluid Mechanics*, 811:168–188, 2017.
- Aashwin A Mishra, Gianluca Iaccarino, and Karthik Duraisamy. Sensitivity of flow evolution on turbulence structure. *Physical Review Fluids*, 1(5):052402, 2016.
- Aashwin Ananda Mishra and Sharath Girimaji. Linear analysis of non-local physics in homogeneous turbulent flows. *Physics of Fluids*, 31(3):035102, 2019.
- Aashwin Ananda Mishra, Karthik Duraisamy, and Gianluca Iaccarino. Estimating uncertainty in homogeneous turbulence evolution due to coarse-graining. *Physics of Fluids*, 31(2): 025106, 2019.
- A Mitra, JP Panda, and HV Warrior. The effects of free stream turbulence on the hydrodynamic characteristics of an auv hull form. *Ocean Engineering*, 174:148–158, 2019.
- Arindam Mitra, Jyoti Prakash Panda, and Hari Vijayan Warrior. Experimental and numerical investigation of the hydrodynamic characteristics of autonomous underwater vehicles over seabeds with complex topography. *Ocean Engineering*, 198: 106978, 2020.
- G Mompean, S Gavrilakis, L Machiels, and MO Deville. On predicting the turbulence-induced secondary flows using nonlinear $k-\epsilon$ models. *Physics of Fluids*, 8(7):1856–1868, 1996.
- Stephane Monte, Pierre Sagaut, and Thomas Gomez. Analysis of turbulent skin friction generated in flow along a cylinder. *Physics of Fluids*, 23(6):065106, 2011.
- JP Panda. A review of pressure strain correlation modeling for reynolds stress models. *Proceedings of the Institution of Mechanical Engineers, Part C: Journal of Mechanical Engineering Science*, page 0954406219893397, 2019.
- JP Panda. A reliable pressure strain correlation model for complex turbulent flows. *Journal of Applied Fluid Mechanics*, 13(4): 1167–1178, 2020.
- JP Panda and HV Warrior. A representation theory-based model for the rapid pressure strain correlation of turbulence. *Journal of Fluids Engineering*, 140(8):081101, 2018.
- JP Panda, HV Warrior, S Maity, A Mitra, and K Sasmal. An improved model including length scale anisotropy for the pressure strain correlation of turbulence. *Journal of Fluids Engineering*, 139(4):044503, 2017.
- JP Panda, A Mitra, AP Joshi, and HV Warrior. Experimental and numerical analysis of grid generated turbulence with and without mean strain. *Experimental thermal and fluid science*, 98:594–603, 2018.
- Jyoti Prakash Panda, Arindam Mitra, and Hari V Warrior. A review on the hydrodynamic characteristics of autonomous underwater vehicles. *Proceedings of the Institution of Mechanical Engineers, Part M: Journal of Engineering for the Maritime Environment*, page 1475090220936896, 2020.
- Jeongyoung Park and Haecheon Choi. Effects of uniform blowing or suction from a spanwise slot on a turbulent boundary layer flow. *Physics of Fluids*, 11(10):3095–3105, 1999.
- Stephen B Pope. *Turbulent flows*, 2001.
- A Posa and E Balaras. A numerical investigation of the wake of an axisymmetric body with appendages. *Journal of Fluid Mechanics*, 792:470–498, 2016.
- Antonio Posa and Elias Balaras. Large-eddy simulations of a notional submarine in towed and self-propelled configurations. *Computers & Fluids*, 165:116–126, 2018.
- Antonio Posa and Elias Balaras. A numerical investigation about the effects of reynolds number on the flow around an appended axisymmetric body of revolution. *Journal of Fluid Mechanics*, 884, 2020.
- Stephen K Robinson. Coherent motions in the turbulent boundary layer. *Annual Review of Fluid Mechanics*, 23(1):601–639, 1991.
- Salim Mohamed Salim, M Ariff, and Siew Cheong Cheah. Wall $y+$ approach for dealing with turbulent flows over a wall mounted cube. *Progress in Computational Fluid Dynamics, an International Journal*, 10(5-6):341–351, 2010.
- William S Saric, David E West, Matthew W Tufts, and Helen L Reed. Experiments on discrete roughness element technology for swept-wing laminar flow control. *AIAA Journal*, 57(2):641–654, 2019.
- AJ Simonsen and P-Å Krogstad. Turbulent stress invariant analysis: Clarification of existing terminology. *Physics of Fluids*, 17(8): 088103, 2005.
- Torbjörn Sjögren and Arne V Johansson. Development and calibration of algebraic nonlinear models for terms in the reynolds stress transport equations. *Physics of Fluids*, 12(6): 1554–1572, 2000.
- Charles G Speziale, Sutanu Sarkar, and Thomas B Gatski. Modelling the pressure–strain correlation of turbulence: an invariant dynamical systems approach. *Journal of fluid mechanics*, 227:245–272, 1991.

- CM Tay, YT Chew, BC Khoo, and JB Zhao. Development of flow structures over dimples. *Experimental Thermal and Fluid Science*, 52:278–287, 2014.
- CMJ Tay, BC Khoo, and YT Chew. Mechanics of drag reduction by shallow dimples in channel flow. *Physics of Fluids*, 27(3):035109, 2015.
- Hari Warrior, Sajo Mathews, Subhendu Maity, and Kaushik Sasmal. An improved model for the return to isotropy of homogeneous turbulence. *Journal of Fluids Engineering*, 136(3), 2014.
- Scott Watkins, Jose Montoya-Segnini, Humberto Bocanegra Evans, Oscar Curet, Serdar Gorumlu, Burak Aksak, Amirkhosro Kazemi, Leonardo Chamorro, and Luciano Castillo. Flow around an autonomous underwater vehicle with bio-inspired coating. *APS*, pages A16–007, 2017.
- Se Youl Won, Qiang Zhang, and Phillip M Ligrani. Comparisons of flow structure above dimpled surfaces with different dimple depths in a channel. *Physics of Fluids*, 17(4):045105, 2005.
- Li Xi. Turbulent drag reduction by polymer additives: Fundamentals and recent advances. *Physics of Fluids*, 31(12):121302, 2019.